journal homepage: www.intl.elsevierhealth.com/journals/cmpb

Simulation of biological ion channels with technology computer-aided design

Santosh Pandey[a,*], *Akwete Bortei-Doku*[b], *Marvin H. White*[b,*]

[a] *Electrical and Computer Engineering, Iowa State University, Ames, IA 50011, USA*
[b] *Department of Electrical Engineering, Lehigh University, Bethlehem, PA 18015, USA*

ARTICLE INFO

Article history:
Received 5 November 2004
Received in revised form
20 May 2005
Accepted 28 August 2006

Keywords:
Ion channel
KcsA
Poisson–Nernst–Planck
SILVACO

ABSTRACT

Computer simulations of realistic ion channel structures have always been challenging and a subject of rigorous study. Simulations based on continuum electrostatics have proven to be computationally cheap and reasonably accurate in predicting a channel's behavior. In this paper we discuss the use of a device simulator, SILVACO, to build a solid-state model for KcsA channel and study its steady-state response. SILVACO is a well-established program, typically used by electrical engineers to simulate the process flow and electrical characteristics of solid-state devices. By employing this simulation program, we have presented an alternative computing platform for performing ion channel simulations, besides the known methods of writing codes in programming languages. With the ease of varying the different parameters in the channel's vestibule and the ability of incorporating surface charges, we have shown the wide-ranging possibilities of using a device simulator for ion channel simulations. Our simulated results closely agree with the experimental data, validating our model.

1. Introduction

Biological ion channels are transmembrane proteins that regulate the ion flux through a cell, and thereby play an integral role in cellular signaling mechanisms [1]. Modeling of ion channels has a long history, but the lack of detailed structural knowledge hampered the progress in this field. With advancements in molecular biology and X-ray diffraction techniques, a lot is now known regarding the structural details of ion channels [2].

Ions in solution execute random Brownian motion, and if an electric field is applied, they acquire drift velocity. It is the interaction between the ions and the electric field in the channel that decides the salient features of an ion channel. The effective electric field is a complicated interplay from various sources including the membrane potential, the charge residues on the wall, the surrounding ions, and the charges induced in the membrane wall by these ions [3].

Among the varied approaches available for ion channel modeling, the most accurate representation of the system is provided by molecular dynamics (MD) simulations, where all the atoms in a system are treated explicitly [4,5]. However, MD simulations are presently limited to simulation times of not more than a few nanoseconds, due to the small timesteps (~femtoseconds) required to resolve individual ion trajectories. Any reliable estimates of steady-state channel currents require simulation time durations of the order of milliseconds, thus preventing an experimental validation of MD simulations [6].

An alternative method is to follow the motion of individual ions using Brownian dynamics simulations [7,8]. Here, it is assumed that the protein structure is fixed and water

* *Corresponding authors*. Tel.: +1 610 758 4421.
E-mail addresses: pandey@iastate.edu (S. Pandey), m.white@lehigh.edu (M.H. White).
0169-2607/$ – see front matter © 2006 Elsevier Ireland Ltd. All rights reserved.
doi:10.1016/j.cmpb.2006.08.007

molecules are treated as a continuum. Collisions between the ions and the surrounding water molecules are mimicked by random fluctuating forces plus an average frictional force. A major advantage of Brownian dynamic approach is the ability to allow direct simulation of ion–ion interaction and calculate an ion's interaction energy with respect to the system during each time step [7]. But this has always been an involved, time-consuming process [9].

Using a mean field approximation, continuum electrostatics provides a rather simplistic alternative to ion channel modeling [10]. It involves solving the Poisson–Nernst–Planck (PNP) equations for the charge distribution inside the channel, and has proven to be very computationally cheap. Even though the PNP method uses a major approximation of reducing the ion–ion interactions to an interaction between an ion and a mean field, its results have shown to be in good agreement with the experimental data [11,12].

In this paper we present a novel method of simulating ion channels based on continuum electrostatics. We have attempted to represent the structure of a KcsA channel as a solid-state device, with its intrinsic material properties similar to that in the realistic case [13,14]. Simulations are performed on a solid-state device simulator, SILVACO International, providing us with the steady-state behavior of the KcsA channel. The simulation results agree well with the available experimental data.

2. Methods

2.1. Poisson–Nernst–Planck (PNP) theory

The PNP approach to ion permeation in membrane channels has been studied in numerous works [10,11,15]. The PNP equations are similar to the drift–diffusion equations that describe the carrier dynamics in semiconductors [16]. The flux J of each ion species is described by the Nernst–Planck (NP) equation, which combines the diffusion due to a concentration gradient with the potential gradient [16,17]:

$$J = -D\left(\nabla n + \frac{zen}{kT}\nabla\phi\right) \quad (1)$$

where D is the diffusion coefficient, z the valency of the ion, e the electronic charge, k the Boltzmann constant, T the temperature, n the concentration of the ion, and Φ is the potential. Also, the Poisson's equation is written as [16,17]:

$$\varepsilon_0\nabla[\varepsilon(r)\nabla\phi(r)] = -\sum_{\text{ions}} zen - \rho_{\text{ex}} \quad (2)$$

where $\varepsilon(r)$ is the dielectric constant at an axial distance, r the sum over all ions gives the total mobile charge, ε_0 the dielectric constant of free space, and ρ_{ex} represents all the external fixed and induced charges. It is to be noted that, realistically, all the quantities in Eqs. (1) and (2) are varying along the ion channel axis [12,13]. This makes it notoriously difficult to obtain any analytical solution of the PNP equations, besides in some very specific cases [10]. However, it is possible to solve Eqs. (1) and (2) iteratively and obtain self-consistent solutions for the potential, concentrations and fluxes of the ions along the channel axis [17]. Even though this paper deals with 1D PNP computations, it has been shown that the PNP equations can be extended to 3D with a more realistic channel representation and even closer fits to the experimental data [12].

2.2. The SILVACO simulator

SILVACO is a solid-state process and device simulator that has the general capabilities for numerical, physically based, 2D and 3D simulations of semiconductor devices [18]. It has two components: ATHENA, which is a 2D process simulation framework with software tools for modeling semiconductor fabrication processes, and ATLAS, which predicts the electrical behavior of semiconductor structures and provides insight into the internal physical mechanisms associated with device operation. ATLAS produces outputs in three forms: the run time output as a guide to the progress of the simulations running, log files storing summaries of the electrical output information, and the solution files storing the data related to the values of the solution variables within the device. The numerous carrier transport models, the availability of different material substrates, and the ability to account for other physical effects (e.g. surface charges, lattice heating, generation and recombination) have added greater flexibility to this device simulator.

Semiconductor device operation is modeled in ATLAS by a set of one to six coupled, non-linear partial-differential equations (PDE) [18]. ATLAS provides numerical solutions of these equations by calculating the values of the unknowns on a mesh of points within the device. The original, continuous model (similar to the PNP equations) is converted to a discrete, non-linear algebraic system by an internal discretization procedure. The sets of PDEs, the mesh and the discretization procedure determine the non-linear algebraic problem to be solved. This is solved using an iterative procedure that refines successive estimates of the solution. Different solution procedures (e.g. Gummel, Newton, or block iteration) exhibit different behavior with respect to convergence, accuracy, efficiency and robustness.

2.3. KcsA ion channel simulations with SILVACO

Based on its structure revealed by X-ray crystallography [2,13], we have built a KcsA channel model as shown in Fig. 1. The potassium channel is modeled here as a transmembrane lumen, surrounded by protein walls and with cylindrical reservoirs of potassium and chloride ions at two ends [4–13]. The channel extends from 10 to 50 Å, with a narrow selectivity filter of radius 1.5 Å and length 12 Å and a wider segment of length 23 Å. The selectivity filter extends into the extracellular space, while the wider segment tapers towards the intracellular space. Each reservoir at either end has a radius of 40 Å and a width of around 8 Å.

To replicate the shape of the KcsA channel, the structure is made of two materials: one to mimic the water continuum that is conducting, and the other to mimic the non-conducting protein walls [15,19]. The dielectric constants ε of the conducting and non-conducting mediums are set as 80 and 2, respectively. The entire device is constructed from 55 rectangular regions, which is the maximum limit for ATLAS [18]. Each conduct-

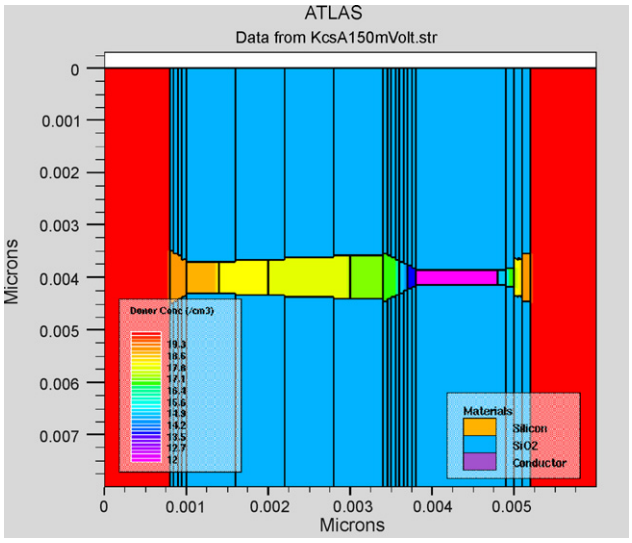

Fig. 1 – The model of a KcsA ion channel built in SILVACO. The channel extends from 10 to 50 Å, with a narrow selectivity filter of radius 1.5 Å and length 12 Å and a wider segment of length 23 Å. The selectivity filter extends into the extracellular space, while the wider segment tapers towards the intracellular space.

ing region has the capability of being defined with its unique material properties. To this end, the carrier doping and their diffusion coefficients are specified in each conducting region as shown in Fig. 2. This allows us to emulate the fact that there are considerably fewer carriers in the vestibule of the channel compared to in the reservoirs. Interestingly, the selectivity filter hardly has four to five ions at one instant [13], which is represented as an undoped region in Fig. 2. After the definition of the device structure, the mesh points are specified to

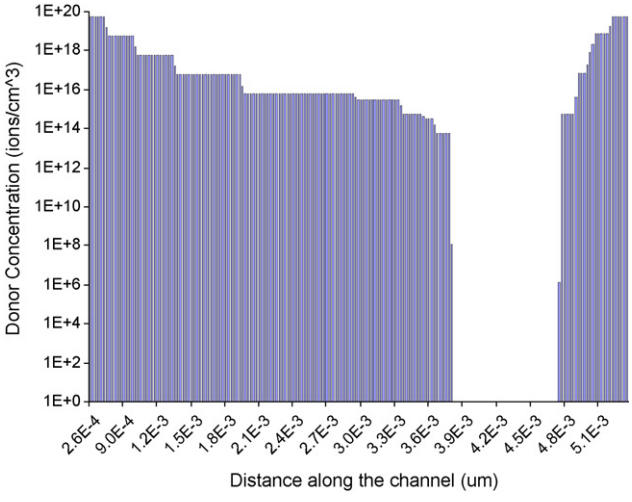

Fig. 2 – The doping profile of the various conducting regions in the KcsA model. The extracellular baths have a symmetric concentration of 100 mM equivalently, while the selectivity filter is left undoped. The profile to chosen to represent the realistic scenario in the vestibule of the channel [13].

denote the locations where solutions are to be determined. The mesh is defined by a series of horizontal and vertical lines and the spacing between them. With a maximum limit of only 9600 mesh nodes in ATLAS [18], it is important to use the mesh lines wisely and in locations which are crucial for the device behavior. Two electrodes, the source and drain, each of length 20 Å are placed at either ends of the reservoirs for applying a potential and measuring the electrodiffusion characteristics of the device.

Despite the fact that ion channels can be modeled as nanoscale electronic devices as discussed above, there are several issues to be addressed in their electrical simulations. The carriers in electronic devices are electrons and holes, while those in ion channels are charged ions bound by hydration shells [10]. The masses and radii of the semiconductor carriers are significantly small compared to those of ions in channels. Furthermore, the diffusion coefficient of electrons is around 500 $cm^2\,s^{-1}$, while that of K^+ ions is around 5×10^{-7} $cm^2\,s^{-1}$. The energy band structure and crystalline structures of solid-state materials is well known, whereas that of liquids is less known. On the brighter side, the drift–diffusion PNP theory still holds for both solid-state devices and ion channels, providing a simplistic, macroscopic study of the flow of electrons and ions alike [15–17]. With this basis, we have incorporated many of the characteristics of ion flow into our channel model. Even though it is difficult take into account the large mass and radii of ions, we have adjusted the diffusion coefficients of electrons in each conducting region to describe the slower motion of ions in a channel's vestibule [19]. Also, the net carrier doping and the degree of ionization is specified in a manner to predict decreased concentrations in the channel's vestibule and to obtain realistic current–voltage plots, as shown in Fig. 2. For this purpose, we have used the fact that the carrier doping density (per cm^3) is given by $n = 10^3 N_{AV} C$, where N_{AV} is the Avogadro's number and C is the concentration of the solution (mol/l). As will be demonstrated in the next section, with these modifications and appropriate mesh definition, it is possible to obtain realistic simulations results.

3. Results

The solid-state KcsA channel model was simulated using the PNP theory under various symmetric bath concentrations and potentials. The discretized PNP equations were solved by ATLAS using Gummel iteration and with each simulation runtime of <30 s.

Figs. 3 and 4 show the potential contours along the channel at a bath concentration of 100 mM and voltages of 100 and 200 mV, respectively. In Fig. 3, for example, a voltage potential of 100 mV was applied to the drain electrode in the reservoir at the right side, while the source electrode at the left side reservoir was kept at ground. The potential drops gradually along the channel, with most of the significant voltage drop occurring within the 12 Å length of narrow selectivity filter. Figs. 5 and 6 plot the electric field contours along the channel axis at 100 and 200 mV, respectively, and a 100 mM bath concentration. The electric field variations can be observed along the channel, with noticeable changes at either mouths of the narrow selectivity filter. The entrance and exit of the channel

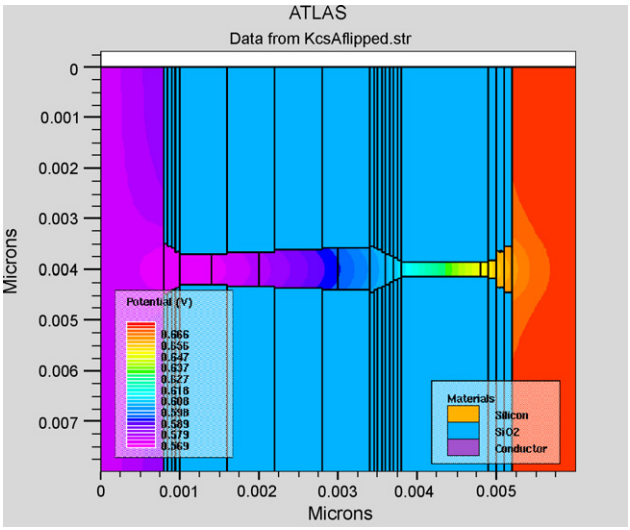

Fig. 3 – The SILVACO contour profile of the potential variation along the channel axis with 100 mV applied across the channel and extracellular bath concentrations of 100 mM.

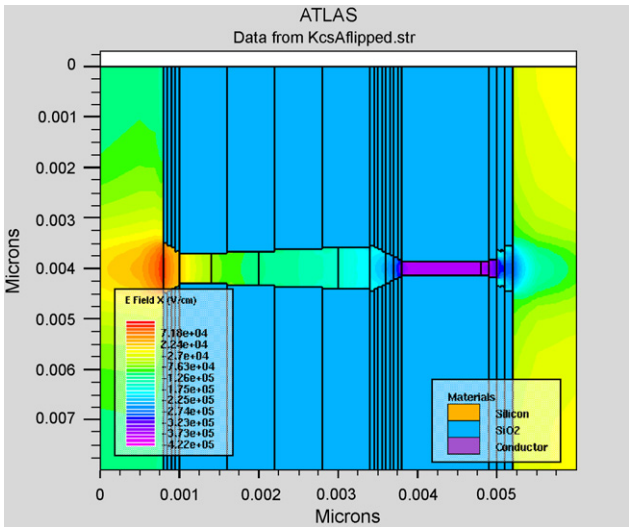

Fig. 5 – The SILVACO contour profile of the electric field variation along the channel axis with 100 mV applied across the channel and extracellular bath concentrations of 100 mM.

are made rounded, as any sharp boundaries cause problems while solving the Poisson's equation and lead to unwanted peaks.

Figs. 7 and 8 plot of the electric fields and potentials, respectively, along the channel for varying drain voltages and a bath concentration of 100 mM. As observed, the simulation program takes into account an inherent built-in potential of the structure, which is around ~0.575 V in this case. The origin of this potential is similar to that of Nernst Potential in ion channels as the SILVACO program considers the same Boltzmann energy distribution of carriers [10]. In this case, the bath concentration is 6×10^{19} cm^{-3} (or 100 mM equivalently) and the inside of the channel has an intrinsic concentration of 10^{10} cm^{-3}. Plugging this in the formula for the built-in potential $V = (kT/q)\ln(C_{bath}/C_{channel})$, we get a value of ~0.575 V. In Figs. 9 and 10, we plot the electric fields and potentials, respectively, along the channel for a fixed drain voltage of 100 mV and varying symmetric bath concentrations. As expected, the built-in potential increases with increasing extracellular concentrations.

In an attempt to check the validity of our model, we compare the current–voltage (IV) characteristics from our simulations with those of experiments [20]. Fig. 11 shows the corresponding IV plots of a KcsA channel at two symmetric bath concentrations of 250 and 500 mM. Using reverse engineering, the material properties of the solid-state KcsA structure

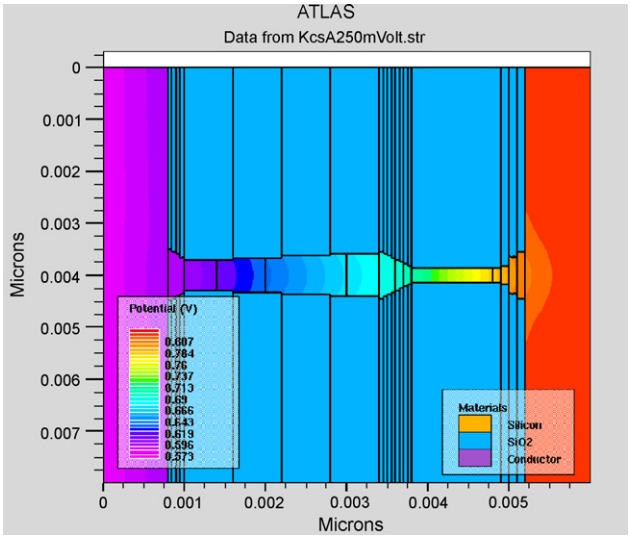

Fig. 4 – The SILVACO contour profile of the potential variation along the channel axis with 200 mV applied across the channel and extracellular bath concentrations of 100 mM.

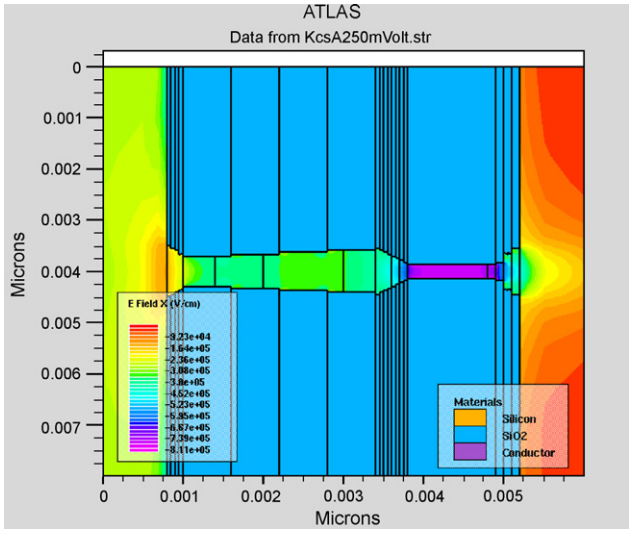

Fig. 6 – The SILVACO contour profile of the electric field variation along the channel axis with 200 mV applied across the channel and extracellular bath concentrations of 100 mM.

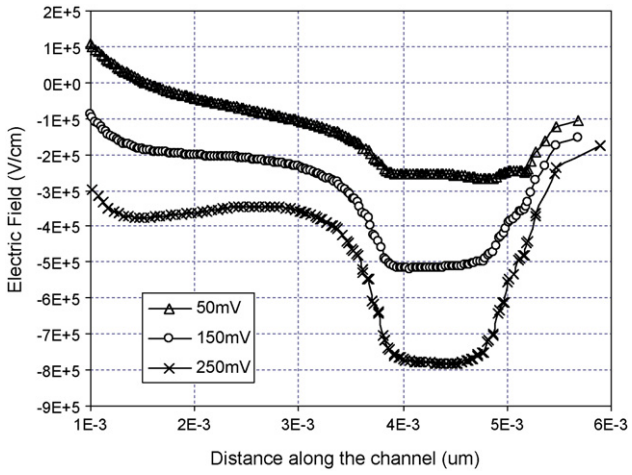

Fig. 7 – Plots of electric field variation along the channel axis at varying voltages applied across the channel and extracellular bath concentrations of 100 mM.

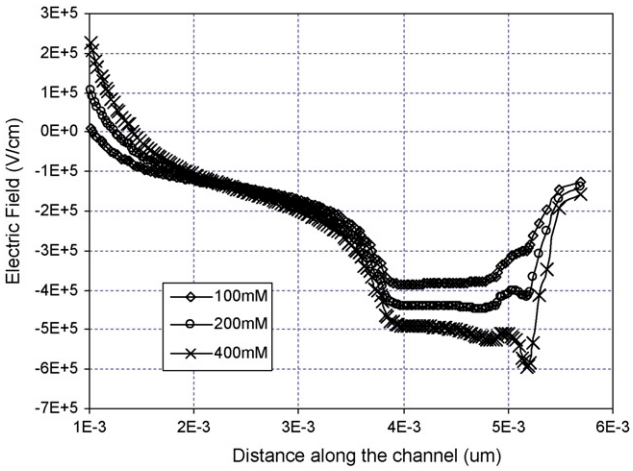

Fig. 9 – Plots of electric field variation along the channel axis at varying extracellular bath concentrations and an applied voltage of 100 mV across the channel. In each case, both the baths are symmetric, having the same concentration.

have been adjusted so as to mimic the realistic ion-channel structure and obtain a good fit between the IV curves. As seen from Fig. 11, the simulated IV curves closely agree with the experimental IV curves until 70 mV. Above this voltage, there is a slight tendency towards saturation in the experimental curves, whereas the simulated IV curves keep rising almost linearly. Nevertheless, this degree of agreement between our simulated results and the experimental IV curves is much better than those reported in the previous literature [9].

Next, we consider the effect of surface charges on the electrical properties of KcsA channels. These surface charges are known to influence the gating, conductance, and toxin-binding effects of KcsA ion-channels, and their actual physical locations are presumed to be in the selectivity filter [21]. Being negatively charged, these surface charges aid the permeation of cations and impede the flow of anions through the KscA channel. Here, we explored the effects of such charges on ion permeation by placing three positive charges in the selectivity filter at the interface of water and protein walls (at 40, 44, and 48 Å in Fig. 2). It is worth mentioning that the surface charges in our simulations are positive (each $Q_{SC} = 10^{14}$ cm^{-2}) since the majority carriers used in our model are electrons. The SILVACO program is versatile in allowing us to incorporate any fixed charges, interface traps, or even bulk traps at the semiconductor–insulator interface and observing their effects on the conduction of a device [18]. Fig. 12 plots the potential variation along the channel with a bath concentration of 100 mM and drain voltages of 0 V, 150 mV and 250 mV. In comparison to its steadily increasing nature in Fig. 7 (with no charges), the axial potential variation in Fig. 12 (with surface charges) has a plateau inside the selectivity filter, with three small humps resulting from the charges at those locations. The simulated IV curves (with and without charges) are plotted in Fig. 13 for a 250 mM bath concentration. Besides the

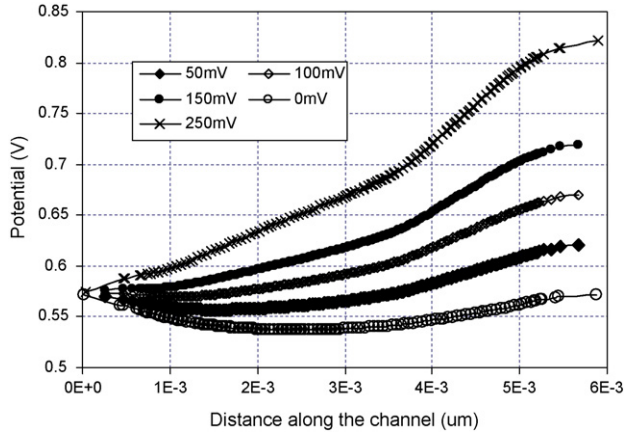

Fig. 8 – Plots of potential variation along the channel axis at varying voltages applied across the channel and extracellular bath concentrations of 100 mM.

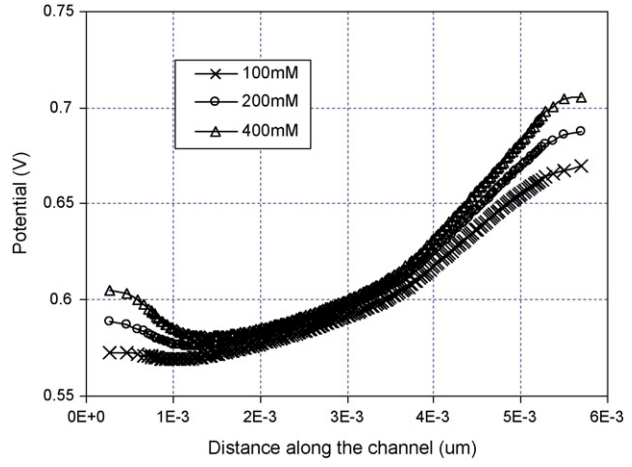

Fig. 10 – Plots of potential variation along the channel axis at varying extracellular bath concentrations and an applied voltage of 100 mV across the channel. In each case, both the baths are symmetric, having the same concentration.

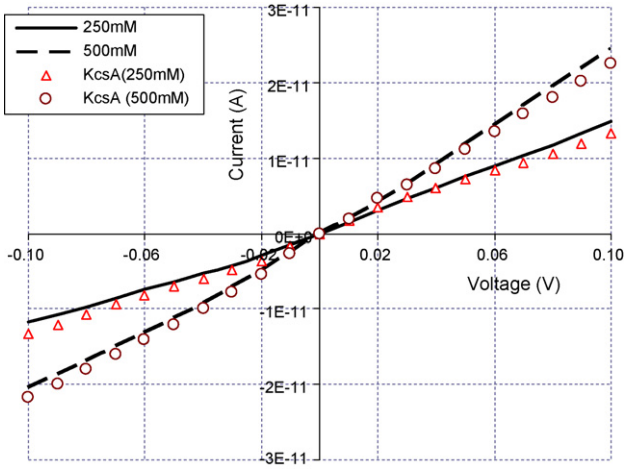

Fig. 11 – The current–voltage characteristics of the KcsA channel model at two different symmetric bath concentrations (250 and 500 mM). Comparison is made between the SILVACO simulated plots (—, 250 mM; – – –, 500 mM) and the experimental data (△, KcsA: 250 mM; ○, KcsA: 500 mM).

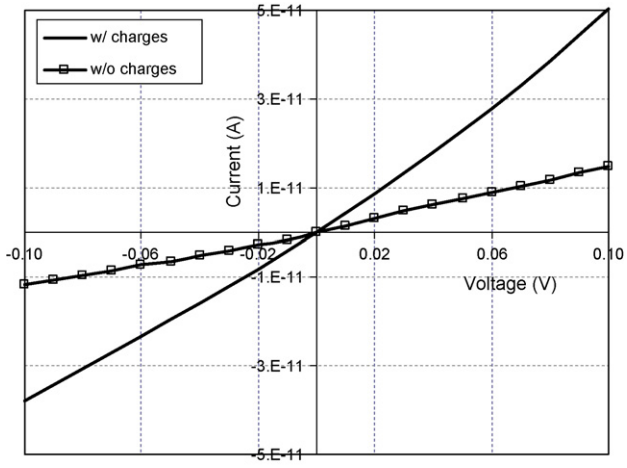

Fig. 13 – The simulated current–voltage characteristics of the KcsA channel model in the presence of surface charges and at two different symmetric bath concentrations (250 and 500 mM). Besides the increase in conductance, there is an enhancement in the majority carrier current and decrease in the minority carrier current. The nature and amount of surface charges is same as that in Fig. 12.

general increase in conductance, there is an added asymmetry in the linearity of the IV curves (in positive and negative voltage ranges) by surface charges. As seen in Fig. 13, the current component due to the majority carriers (electrons) is enhanced much more compared to that due to the minority carriers (holes) owing to the attractive and repulsive forces, respectively, exerted by the surface charges.

4. Discussion

We have demonstrated the possibility of representing a KcsA channel as a solid-state device, and employing a device simulator, SILVACO, to simulate its electrical characteristics. With a goal to mimic the realistic and computationally feasible scenario inside an ion channel, we created a model with well-adjusted material parameters and employed SILVACO to obtain self-consistent solutions of the axial potential and ion fluxes. The simulated IV curves closely match the available experimental results, supporting the validity of the model.

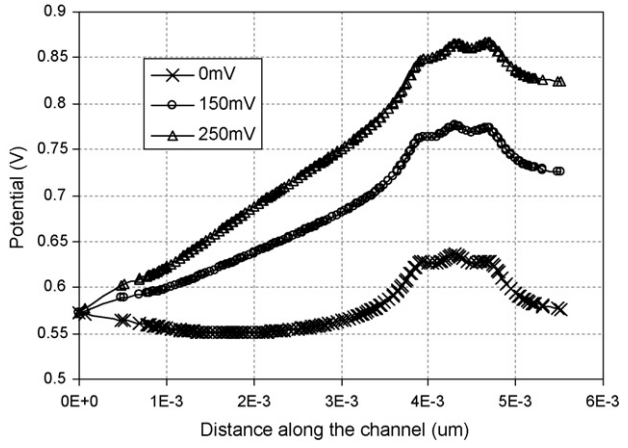

Fig. 12 – Plots of potential variation along the channel axis at varying voltages applied across the channel, in the presence of surface charges, and extracellular bath concentrations of 100 mM. Three pairs of charges (each $Q_{SC} = 10^{14}$ cm^{-2}) are located inside the selectivity filter at the interface between the water and protein walls (at 40, 44, and 48 Å in Fig. 2).

Besides giving insight into the general ion permeation mechanisms in a channel's vestibule, the simulation results do open exciting opportunities to extend this work. Additional features can be incorporated in the model to bridge the gap between the nature of a semiconductor–insulator and a water–protein wall interface. In solid-state devices, the interface between a semiconductor and an overlying insulator is sharp and abrupt, while the dielectric boundary at a channel's water–protein wall interface is not so distinctly defined. This dielectric boundary and its curvature is important in deciding an ion's potential energy, which varies as $1/\varepsilon_{water}$ in the baths and as $1/\varepsilon_{protein}$ inside the channel [22]. Even though the precise value of $\varepsilon_{protein}$ is not crucial, it would better our model to put an additional protein region ($\varepsilon_{protein} \cong 10$) at the dielectric boundary to smoothen the sharp water–protein wall interface. Also, it is suspected that the dielectric constant of water decreases inside the channel, and recently Monte Carlo simulations have shown that lowering its dielectric constant in a channel's vestibule alters a channel's selectivity for different ions [5]. Studies can be performed to investigate the effects of changing ε_{water} on the channel permeation and its selectivity for monovalent or divalent ions.

Although our model is based on macroscopic drift–diffusion computations, they do describe the experimental IV data surprisingly well. It is, however, tempting to be able to perform simulations at molecular and atomistic levels (Monte Carlo and Brownian dynamics) with the computational ease of PNP programs [19]. In this context, a common platform can

be built which has the capability of running molecular-level simulations for a short timeframe, inferring the ion-transport parameters, and feeding them to the SILVACO program to calculate the ion fluxes within reasonable time. Such a hybrid model would blend the accurate predictions of molecular-level simulations with the computationally cheap macroscopic flux calculations.

REFERENCES

[1] M. Schumacher, J. Adelman, Ion channels: an open and shut case, Nature 417 (2002) 501–502.

[2] Y. Jiang, A. Lee, J. Chen, V. Ruta, M. Cadene, B. Chait, R. Mackinnon, X-ray structure of a voltage-dependent K^+ channel, Nature 423 (2003) 33–41.

[3] D. Levitt, Electrostatic calculations for an ion channel: energy and potential profiles and interactions between ions, Biophys. J. 22 (1978) 210–218.

[4] P. Graf, M. Kurnikova, R. Coalson, A. Nitzan, Comparison of dynamic lattice Monte Carlo simulations and the dielectric self-energy Poisson–Nernst–Planck continuum theory for model ion channels, J. Chem. Phys. B 108 (2003) 2006–2015.

[5] D. Boda, T. Varga, D. Henderson, D. Busath, W. Nonner, D. Gillespie, B. Eisenberg, Monte Carlo simulation study of a system with a dielectric boundary: application to calcium channel selectivity, Mol. Simul. 30 (2004) 89–96.

[6] B. Corry, S. Kuyucak, S.-H. Chung, Dielectric self-energy in Poisson–Boltzmann and Poisson–Nernst–Planck models of ion channels, Biophys. J. 84 (2003) 3594–3606.

[7] S.-H. Chung, M. Hoyles, T. Allen, S. Kuyucak, Study of ionic currents across a model membrane channel using Brownian dynamics, Biophys. J. 75 (1998) 793–809.

[8] S. Aboud, D. Marreiro, M. Saraniti, R.S. Eisenberg, Brownian dynamics simulations of transport properties in potassium ion channels, in: Proceedings of the 2004 Nanotechnology Conference and Trade Show 1, 2004, pp. 135–138.

[9] C. Miller, A. Asenov, S. Roy, Brownian dynamics based particle mesh simulations of ionic solutions and channels, in: Proceedings of the2003 Nanotechnology Conference and Trade Show 3, 2003, pp. 431–434.

[10] B. Hille, Ionic Channels of Excitable Membranes, Sinauer Associates Inc., Cambridge, NY, 1992.

[11] U. Hollerbach, D. Chen, D. Busath, B. Eisenberg, Predicting function from structure using the Poisson–Nernst–Planck equations: sodium current in the Gramicidin-A channel, Langmuir 16 (2000) 5509–5514.

[12] A. Cardenas, R. Coalson, M. Kurnikova, 3D Poisson–Nernst–Planck theory studies: Influence of membrane electrostatics on Gramicidin A channel conductance, Biophys. J. 79 (2000) 80–93.

[13] D. Doyle, J. Cabral, R. Pfuetzner, A. Kuo, J. Gulbis, S. Cohen, B. Chait, R. MacKinnon, The structure of the potassium channel: molecular basis of K^+ conduction and selectivity, Science 280 (1998) 69–77.

[14] A. Burykin, C. Schutz, J. Villa, A. Warshel, Simulations of ion current in realistic models of ion channels: the KcsA postassium channel, Proteins: Struct. Funct. Genet. 47 (2002) 265–280.

[15] R. Eisenberg, From structure to function in open ionic channels, J. Membr. Biol. 171 (1999) 1–24.

[16] S.M. Sze, Physics of Semiconductor Devices, John Wiley & Sons Inc., 1981, pp. 75–93.

[17] W. Nonner, R. Eisenberg, Ion permeation and glutamate residues linked by Poisson–Nernst–Planck theory in L-type calcium channels, Biophys. J. 75 (1998) 1287–1305.

[18] Atlas, User's Manual: Device Simulation Software, SILVACO International Inc., 1998.

[19] S. Natarajan, S. Varma, Y. Tang, S. Parker, J. Mashl, E. Jakobsson, Toward an integrated computational environment for multiscale computational design of nanoscale ion channel semiconductors, in: Proceedings of the 2004 Nanotechnology Conference and Trade Show 1, 2004, pp. 147–150.

[20] D. Meuser, H. Splitt, R. Wagner, H. Schrempf, Exploring the open pore of the potassium channel from *Streptomyces lividans*, FEBS Lett. 462 (1999) 447–452.

[21] L. Bashford, G. Alder, C. Pasternak, Fluctuations of surface charge in membrane pores, Biophys. J. 82 (2002) 2032–2040.

[22] T. Bastug, S. Kuyucak, Role of the dielectric constants of membrane proteins and channel water in ion permeation, Biophys. J. 84 (2003) 2871–2882.